JACS
JOURNAL OF THE AMERICAN CHEMICAL SOCIETY

Communication

pubs.acs.org/JACS

DNA-Directed Assembly of Gold Nanohalo for Quantitative Plasmonic Imaging of Single-Particle Catalysis

Kun Li,[†] Kun Wang,[†] Weiwei Qin,[†] Suhui Deng,[†] Di Li,*[,†] Jiye Shi,[†,‡] Qing Huang,[†] and Chunhai Fan[†]

[†]Division of Physical Biology & Bioimaging Center, Shanghai Synchrotron Radiation Facility, CAS Key Laboratory of Interfacial Physics and Technology, Shanghai Institute of Applied Physics, Chinese Academy of Sciences, Shanghai 201800, China

[‡]UCB Pharma, Slough, SL1 14EN Berkshire, U.K.

Supporting Information

ABSTRACT: Plasmonic imaging under a dark-field microscope (DFM) holds great promise for single-particle analysis in bioimaging, nanophotonics, and nanocatalysis. Here, we designed a DNA-directed programmable assembly strategy to fabricate a halo-like Au nanostructure (nanohalo) that couples plasmonic large gold nanoparticles (L-AuNPs) with catalytically active small AuNPs (S-AuNPs) in a single nanoarchitecture. Catalytic reaction occurring on S-AuNPs changes its permittivity, which results in a significant variation of the plasmonic resonance of the nanohalo. Hence, we can indirectly monitor catalytic reactions on a single nanohalo under DFM, on the basis of which we have obtained quantitative information on both nanocatalysis and catalyst poisoning. Our study thus provides a cost-effective means to quantitatively study metal NP-based catalysis at single-particle level.

The ability to assemble different functional building blocks to a hierarchical nanoarchitecture is highly desirable for nanoelectronics, nanophotonics, and intelligent sensing. Besides the aesthetic value of well-defined ordered structure, nanoarchitectures with multiple functions provide new tools to explore physical and chemical properties at the nanoscale.[1] Gold nanoparticles (AuNPs) have garnered considerable attention in the last decades due to their excellent biocompatibility and prominent plasmonic and catalytic properties.[2] In particular, local surface plasmon resonance (LSPR) of AuNPs involves the collective oscillation of dielectrically confined conduction electrons, which enables the confinement of light to regions with subwavelength dimensions. Therefore, Au-based hierarchical nanoarchitectures have been popularly explored for studying new plasmonic phenomenon[3] and for applications such as bioimaging,[4] targeted cargo delivery,[5] and photothermal therapy.[6]

LSPR of plasmonic NPs is highly sensitive to the refractive index or dielectric constant of surrounding media, thereby holding great promise for monitoring the states of plasmonic nanocatalysts during catalysis.[7] For example, Mulvaney demonstrated the possibility of direct observing of a redox reaction on single gold nanorod using DFM.[8] However, owing to the limit of CCD sensitivity, DFM could only capture the scatter light from large AuNPs (L-AuNPs) with diameters over 50 nm (d > 50 nm), which is often catalytically inactive. Therefore, it is highly desirable to develop a new way to comprise the two properties of AuNPs, the plasmonic property for L-AuNPs, and the catalytic property for small, catalytically active AuNPs (S-AuNPs, d < 15 nm).

One possible solution is to assemble plasmonic NPs and nanocatalysts into a multicomponent nanoarchitecture, dubbed nanoantenna, for indirect monitoring of catalytic processes.[9] For example, Larsson[10] and Alivisatos[11] fabricated nanoantenna composed of Au plasmonic NPs and Pd nanocatalysts by using nanolithography, on the basis of which they plasmonically studied gas sensing and gas-phase catalysis. Despite the elegance of their work, the use of top-down nanolithography is cost-intensive and limits its application in studying NP-based catalysis in solution.[12] In this work, we report on a DNA-based bottom-up approach to programmable construct a nanohalo architecture that can indirectly monitor solution-phase catalysis at single-particle level. Specially, the plasmonic L-AuNPs and catalytic S-AuNPs are brought to the close proximity by DNA self-assembly. The locally enhanced electromagnetic field in the gap between L- and S-AuNPs allows indirect and sensitive monitoring of the catalytic reaction, which provides ready extraction of physicochemical parameters for quantitative understanding of AuNP-based catalysis.

The Au nanohalo was prepared by the DNA-directed self-assembly of AuNPs of different diameters (Figure 1A). Briefly, AuNPs with diameters of 50 and 13 nm were modified with thiolated oligonucleotides with complementary sequences. Of note, the choice of AuNPs (13 nm) as S-NPs is a compromise between catalytic activity and plasmon-induced electromagnetic field enhancement (see part 3 and Figure S1, Supporting Information). DNA plays two critical roles in the hierarchical assembly: controlling the distance and modulating the catalytic activities. The distance (~9 nm) between L- and S-AuNPs was controlled by the length of hybridized oligonucleotides (20 bp), a short distance that favors strong plasmon coupling (Figure 1B). The catalytic activity of AuNPs in nanohalo was also modulated by rationally tuning the surface density of modified oligonucleotides on L- and S-NPs (Figure 1C). The L-NPs with dense modification are catalytically inert, while S-NPs with loose modification are still active. As a result, the catalytic activity of Au nanohalo is exclusively contributed by the loosely modified S-NPs (Figure 1C, inset). We carried out finite-difference time-domain (FDTD) simulations to calculate the enhanced electromagnetic field in Au nanohalo. The electric

Received: January 12, 2015
Published: March 27, 2015

DOI: 10.1021/jacs.5b00324
J. Am. Chem. Soc. 2015, 137, 4292−4295

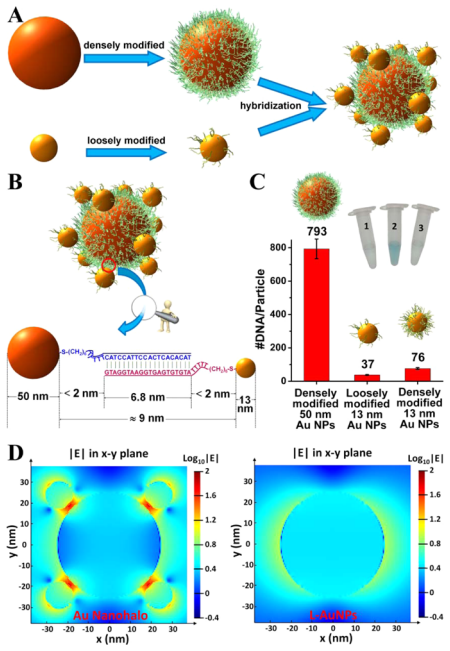

Figure 1. (A) Synthetic scheme for the preparation of Au nanohalo through the self-assembly of AuNPs of different diameters modified with complementary oligonucleotides. (B) Schematic demonstration of the distance between L- and S-AuNPs, which is determined by the rationally designed length of oligonucleotides. (C) Number of oligonucleotides per particle of different kinds of L- and S-AuNPs. Inset shows the colored product that is catalyzed by L- and S-AuNPs that loaded different amounts of oligonucleotides, respectively, as tested by a HRP-cascaded colorimetric reaction. (D) Electromagnetic finite-difference time-domain (FDTD) simulation of the local electric fields enhancement (Log |E|) of the Au nanohalo (left) and L-AuNPs (right) at the $X-Y$ plane. $|E| = |E_{local}/E_{in}|$, where E_{local} and E_{in} represent the amplitude of the local and incident electric fields, respectively.

field intensity (|E|) in the gap between L- and S-AuNPs was found to have ~15-fold enhancement as compared with that on the surface of L-AuNPs (Figure 1D). The strongly enhanced plasmon near-field in the gap can sense the change in the dielectric function of the proximal S-NPs. Therefore, small change in the permittivity of S-AuNPs should bring about significant change of plasmonic resonance of L-AuNPs, which makes it possible to monitor catalytic reactions occurring on S-AuNPs.

The structure and its LSPR response of the as-prepared nanohalo were characterized by TEM and DFM, respectively (see part 4, Figure S2, Supporting Information). Of note, 3D Au nanohalo was rearranged to 2D-packed structures owing to the capillary forces during the drying process on TEM grid (Figure S2A). The ratio of S-/L-NPs ranged from 11−14 in 200 randomly counted particles (Figure S2B). The as-prepared Au nanohalo was then attached on ITO for DFM measurements. Figure S2, panels C and D of the Supporting Information show representative high-resolution SEM and DFM images of an individual Au nanohalo with an S-/L- ratio of 12 (colocalization of this Au nanohalo in SEM and DFM images, see Figure S3, Supporting Information). The Au nanohalo scattered yellow light with plasmon band at 616.45 nm (Figure S2E), while L-NPs scattered green light with the plasmon band at 557.78 nm (Figure S4).

Metal NPs are important catalysts for many chemical transformations due to their size-induced high surface-to-volume ratio and high chemical potentials. However, owing to the complexity of heterogeneous reactions, detailed physicochemical information obtained on heterogeneous catalysts is scarce. Typically, heterogeneous catalytic processes involve the contact of gas or liquid reactant with nanocatalysts. During catalysis, several physicochemical processes occurred successively on nanocatalysts including adsorption of reactants on catalysts, electron transfer between donor and acceptor molecules, and detachment of products from catalysts to eventually catalyst poisoning that ends the reaction.[13] All these processes are associated with the permittivity changes of the plasmonic nanocatalysts; therefore, we could correlate the plasmonic band shifts of the nanohalo with the state of AuNPs during catalysis and derive quantitative information.

We thereby employed this nanohalo as a plasmonic probe to monitor a catalytic reaction. Because of the difficulty of synthesis of monovalent-modified L-NPs, currently we are unable to obtain Au nanohalo with only one S-NP to observe single NP catalytic dynamics. In addition, DNA functionalization intrinsically influenced the catalytic properties of nanocatalysts, which compromises the value of the present method.[14] Future development in DNA nanotechnology, for example, addressable DNA origami,[15] may help to synthesis nanohalo with distinct one catalytic NP, however, may still not to exclude the influence of DNA modifications to the catalytic actives.

We chose an AuNPs-catalyzed redox reaction between glucose and O_2 (eq 1) as a model system (for reasons for choosing this reaction, see part 5, Supporting Information).

$$\text{glucose} + O_2 \xrightarrow{\text{AuNPs}} \text{gluconic acid} + H_2O_2 \quad (1)$$

The LSPR spectrum of the Au nanohalo was monitored during the catalytic process. At $t = 0$ min, glucose solution was injected as an electron source to a final concentration of 0.5 M, and LSPR spectrum of this nanohalo was measured (Figure 2A). Upon the addition of glucose, we observed an immediate red-shift of 2.52 nm, followed by a rapid blue-shift of 6.88 nm

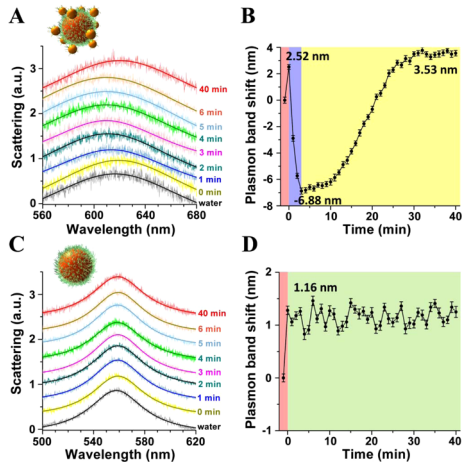

Figure 2. (A) LSPR spectra and (B) the corresponding plasmonic band peak shifts of one Au nanohalo during the catalytic reaction. (C) LSPR spectra and (D) the corresponding plasmon band peak shifts of one L-NPs along the catalytic process under same experimental condition. LSPR spectra were collected by DFM with a time interval of 1 min and then fitted by Lorentz curve to determine the peak position. Error bars in panels B and D represented the deviations coming from the Lorentzian fitting procedure.

DOI: 10.1021/jacs.5b00324
J. Am. Chem. Soc. 2015, 137, 4292−4295

in about 2 min, then another red-shift of 3.53 nm in about 40 min (Figure 2B). In a control experiment, we also analyzed the plasmonic band shifts of L-NPs under the same experimental conditions (Figure 2C) and observed only an initial red-shift of 1.16 nm (Figure 2D).

In catalytic reactions, interactions of reactant with the surface solid catalyst are often decisive. Chemisorption of reactants on nanocatalysts plays a critical role for catalytic performance.[16] It is still a challenge to obtain quantitative results of chemisorption under real reaction conditions.

We speculate that the discontinuous up and down in plasmonic band ($\Delta\lambda$) of Au nanohalo in Figure 2, panel B reflects the different physicochemical process of nanocatalysts in catalysis. Heterogeneous catalysis reaction is activated by the contact of reactants with the surface of catalyst; we thereby assume that the initial 2.52 nm red-shift is attributed to adsorption of glucose on S-NPs. To confirm that, we investigated the relationship between the refractive index of surrounding medium (n), the plasmon bandshift ($\Delta\lambda$), and the change of glucose concentration ($\Delta c_{glucose}$). The sensitivity factors, $\Delta\lambda/\Delta n$, were estimated from the slope of plasmonic response in four different solvents and estimated to be 106.77 nm RIU^{-1} for Au nanohalo (Figure 3A) and 88.26 nm RIU^{-1}

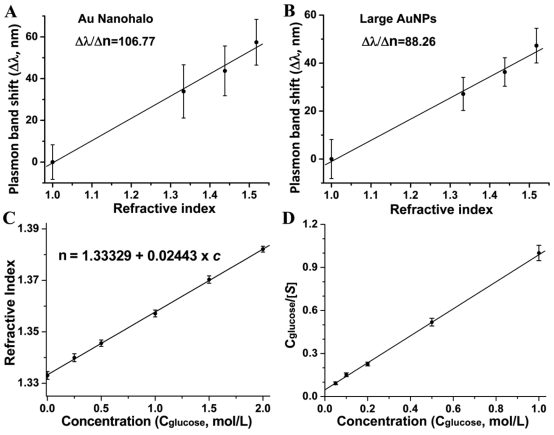

Figure 3. Plots of plasmonic band peak of individual (A) Au nanohalo and (B) L-AuNPs versus refractive index (n) of four different solvents (air (n = 1), water (n = 1.333), ethylene glycol (n = 1.438), and immersion oil (n = 1.518)). Error bars are the standard deviations of 12 signals. (C) Plot of refractive index (n) versus bulk concentration of glucose. The refractive index was obtained from Abbe refractometer. Error bars are the standard deviations of three signals. (D) Langmuir adsorption isotherm of glucose on Au nanohalo. $c_{glucose}$ is the concentration of glucose in bulk solution; [S] is the concentration of glucose molecules that adsorbed on single Au nanoparticle surface. The error bars represent the error in determining of [S] by plasmon band shifts.

for L-NPs (Figure 3B), respectively. Although the signals in Figure 3, panels A and B obtained from 12 individual NPs show different plasmonic response, the slopes remained constant, which indicate that the sensitivity factor is an intrinsic character of their structure (see part 6 and Figure S5, Supporting Information). The concentration factor, $\Delta n/\Delta c_{glucose}$, was calculated from Abbe refractometer by measuring the refractive index at different glucose concentrations and estimated to be 0.02443 (Figure 3C). Therefore, the relationship between $\Delta\lambda$ and $\Delta c_{glucose}$ follows $\Delta\lambda = 2.60839\Delta c_{glucose}$ for Au nanohalo and $\Delta\lambda = 2.15619\Delta c_{glucose}$ for L-AuNPs. We thereby assigned the initial 2.52 nm red-shift in Figure 2, panel B to the change of the refractive index of surroundings from pure water to 0.97 M of glucose or the adsorption of 0.97 M glucose on Au nanohalo. The calculated concentration of surface adsorbed glucose is, however, almost twice concentrated than that in bulk solution (0.5 M), which suggests an enrichment of glucose on Au nanohalo. We thus defined the concentration of surface adsorbed glucose at catalytic sites as [S]; the relationship between $\Delta\lambda$ and surface adsorbed reactant was changed to $\Delta\lambda = 2.60839$[S]. However, for the L-NPs, the 1.16 nm of red-shift in Figure 2, panel D corresponds to 0.54 M of glucose adsorption, only slightly higher than in bulk solution (0.5 M), which further confirms that L-NPs are catalytically inert.

The [S] dependence of $\Delta\lambda$ enables us to quantitatively analyze the chemisorption of glucose on Au nanohalo. By employing Langmuir−Hinshelwood mechanism to simulate this catalysis, we obtained $[S_m] = 1.06 \pm 0.05$ M, $K_{ads} = 20.90 \pm 3.93$ M^{-1} (Figure 3, panel D and part 7, Supporting Information). We calculated the number of glucose adsorbed on each S-NPs (N_{ads}) as 302 (see part 7, Supporting Information). FDTD simulation suggested that the adsorption of 302 glucose molecules would lead to a 2.14 nm of red-shift (Figure S6), similar to but slightly lesser than the experimentally obtained 2.52 nm, which indicates that glucose in bulk solution also contributes to the plasmonic of Au nanohalo to a lesser extent. Of note, the temporal resolution of present DFM setup is 1 min, thereby only few plasmonic band shift were recorded in the fast adsorption process. Introducing a supercontinuum laser as light source could improve the temporal resolution down to 10 ms,[17] which might provide sufficient adsorption information. Despite the presence of these constraints, the present experimental results fit well with numerical stimulation, which confirms the validity of our method.

In heterogeneous redox reactions, following chemisorption of reactant on catalyst, donor and acceptor molecules should transfer electrons on the surface of catalysts. According to microelectrode model,[18] the metal nanocatalyst behaves as an electron reservoir that couples two redox reactions. Hence, we assigned the rapid blue-shift of 6.88 nm and slow red-shift of 3.53 nm to the charging and discharging of S-NPs, respectively. We estimated that ∼11 833 electrons are injected in 3 min, or 66 electrons per second (see part 8, Supporting Information).[8,19] Interestingly, the discharging process (red-shift) is much slower than the rapid charging process (blue-shift). Previous work, however, suggested that rate-determining step of this reaction is the oxidation of adsorbed glucose, while the reduction of O_2 is fast.[20] In our condition, the concentration of glucose (0.5 M) is much higher than that of dissolved oxygen. Therefore, we suggest that the initial dissolved oxygen is quickly reduced by glucose and O_2 in air is then redissolved to the reaction solution and diffuses to Au nanocatalysts to accept the excess of stored electrons, which will result in the retarded discharging.[8]

Catalyst deactivation, or the loss of catalytic activity, is a general problem in heterogeneous catalysis. Catalyst poisoning, the chemisorption of reactants, products, or impurities on active sites, has a large contribution.[21] Indeed, our previous work suggested that catalytic product gluconic acid was adsorbed on Au nanocatalyst surfaces, resulting in catalyst poisoning.[22] Significantly, the plasmonic band of Au nanohalo in Figure 2, panel B does not shift back to its original position after 40 min of reaction, instead, another 3.53 nm of red-shift.

DOI: 10.1021/jacs.5b00324
J. Am. Chem. Soc. 2015, 137, 4292−4295

Accordingly, the catalytic activity of Au nanohalo (in solution) is also diminished after 40 min (Figure S7). We thus consider that the 3.53 nm of red-shift should come from the surface-adsorbed gluconic acid (see part 9 and Figure S8, Supporting Information). Quantitative analysis also revealed that 97.5% of gluconic acid is detached from the AuNPs' surface in each turnover and the remaining 2.5% molecules passivate the catalyst (see part 9, Supporting Information), which eventually results in the poisoning.

Having established single-particle analysis for glucose catalysis using Au nanohalo, we further demonstrate that this is a generic approach to study catalysis on nanocatalysts (see part 10 and Figure S9, Supporting Information). Since the principle of indirect monitoring is the sensing of LSPR response induced by changes of surface coverage and charging state of catalysts, there is no limitation to the other catalysts and catalytic reaction.

In summary, we have constructed a halo-like Au nano-architecture that integrates plasmonic and catalytic properties of AuNPs. The close proximity of large and small NPs in the Au nanohalo results in a confinement and enhancement of local electromagnetic field. Hence, catalytic reactions occurring on S-AuNPs changes its permittivity, which leads to significant changes of the plasmonic resonance of the Au nanohalo. Our work extends the concept of plasmonic nanoantenna to monitor liquid-phase catalytic reactions and provides a cost-effective alternative to study a wide range of catalytic reactions, especially in homogeneous solution.

■ ASSOCIATED CONTENT

Supporting Information

Experimental details and supplementary discussion and figures. This material is available free of charge via the Internet at http://pubs.acs.org.

■ AUTHOR INFORMATION

Corresponding Author

*lidi@sinap.ac.cn

Notes

The authors declare no competing financial interest.

■ ACKNOWLEDGMENTS

This work was supported by the National Basic Research Program of China (973 program, 2013CB932803, 2012CB825800, and 2013CB933800), NSFC (21222508, 3108JC1422600, 21329501, 61378062, 21390414, 91313302), the Shanghai Municipal Commission for Science and Technology (13QH1402300), and Youth Innovation Promotion Association, CAS. We would like to dedicate this paper to Professor Qing Huang, who unfortunately passed away during the reviewing process. Qing Huang played an essential role in the research described here and is greatly missed.

■ REFERENCES

(1) (a) Rossner, C.; Vana, P. *Angew. Chem., Int. Ed.* **2014**, *53*, 12639. (b) Tan, S. J.; Campolongo, M. J.; Luo, D.; Cheng, W. L. *Nat. Nanotechnol.* **2011**, *6*, 268. (c) Nguyen, T. D.; Tran, T. H. *RSC Adv.* **2014**, *4*, 916. (d) Cheng, W. L.; Hartman, M. R.; Smilgies, D. M.; Long, R.; Campolongo, M. J.; Li, R. P.; Sekar, K.; Hui, C. Y.; Luo, D. *Angew. Chem., Int. Ed.* **2010**, *49*, 380. (e) Cheng, W. L.; Campolongo, M. J.; Cha, J. J.; Tan, S. J.; Umbach, C. C.; Muller, D. A.; Luo, D. *Nat. Mater.* **2009**, *8*, 519. (f) Sebba, D. S.; Lazarides, A. A. *J. Phys. Chem. C* **2008**, *112*, 18331. (g) Shi, D. W.; Song, C.; Jiang, Q.; Wang, Z. G.; Ding, B. Q. *Chem. Commun.* **2013**, *49*, 2533. (h) Xiong, W.; Sikdar, D.; Yap, L. W.; Premaratne, M.; Li, X. Y.; Cheng, W. L. *Nanoscale* **2015**, *7*, 3445.

(2) (a) Barrow, S. J.; Wei, X. Z.; Baldauf, J. S.; Funston, A. M.; Mulvaney, P. *Nat. Commun.* **2012**, 1275. (b) Anker, J. N.; Hall, W. P.; Lyandres, O.; Shah, N. C.; Zhao, J.; Van Duyne, R. P. *Nat. Mater.* **2008**, *7*, 442. (c) Li, Y.; Jing, C.; Zhang, L.; Long, Y. T. *Chem. Soc. Rev.* **2012**, *41*, 632.

(3) (a) Gandra, N.; Abbas, A.; Tian, L. M.; Singamaneni, S. *Nano Lett.* **2012**, *12*, 2645. (b) Barrow, S. J.; Funston, A. M.; Wei, X. Z.; Mulvaney, P. *Nano Today* **2013**, *8*, 138.

(4) Li, K.; Qin, W. W.; Li, F.; Zhao, X. C.; Jiang, B. W.; Wang, K.; Deng, S. H.; Fan, C. H.; Li, D. *Angew. Chem., Int. Ed.* **2013**, *52*, 11542.

(5) Wei, M.; Chen, N.; Li, J.; Yin, M.; Liang, L.; He, Y.; Song, H. Y.; Fan, C. H.; Huang, Q. *Angew. Chem., Int. Ed.* **2012**, *51*, 1202.

(6) Jain, P. K.; El-Sayed, I. H.; El-Sayed, M. A. *Nano Today* **2007**, *2*, 18.

(7) (a) Shi, L.; Jing, C.; Ma, W.; Li, D. W.; Halls, J. E.; Marken, F.; Long, Y. T. *Angew. Chem., Int. Ed.* **2013**, *52*, 6011. (b) Xie, W.; Walkenfort, B.; Schlucker, S. *J. Am. Chem. Soc.* **2013**, *135*, 1657. (c) Heck, K. N.; Janesko, B. G.; Scuseria, G. E.; Halas, N. J.; Wong, M. S. *J. Am. Chem. Soc.* **2008**, *130*, 16592. (d) Shan, X. N.; Diez-Perez, I.; Wang, L. J.; Wiktor, P.; Gu, Y.; Zhang, L. H.; Wang, W.; Lu, J.; Wang, S. P.; Gong, Q. H.; Li, J. H.; Tao, N. J. *Nat. Nanotechnol.* **2012**, *7*, 668. (e) Seo, D.; Park, G.; Song, H. *J. Am. Chem. Soc.* **2012**, *134*, 1221.

(8) Novo, C.; Funston, A. M.; Mulvaney, P. *Nat. Nanotechnol.* **2008**, *3*, 598.

(9) (a) Langhammer, C.; Larsson, E. M. *ACS Catal.* **2012**, *2*, 2036. (b) Liu, N.; Wen, F. F.; Zhao, Y.; Y. Wang, M.; Nordlander, P.; Halas, N. J.; Alu, A. *Nano Lett.* **2013**, *13*, 142.

(10) (a) Larsson, E. M.; Langhammer, C.; Zoric, I.; Kasemo, B. *Science* **2009**, *326*, 1091. (b) Langhammer, C.; Larsson, E. M.; Kasemo, B.; Zoric, I. *Nano Lett.* **2010**, *10*, 3529.

(11) (a) Liu, N.; Tang, M. L.; Hentschel, M.; Giessen, H.; Alivisatos, A. P. *Nat. Mater.* **2011**, *10*, 631. (b) Tang, M. L.; Liu, N.; Dionne, J. A.; Alivisatos, A. P. *J. Am. Chem. Soc.* **2011**, *133*, 13220.

(12) Vaughan, O. *Nat. Nanotechnol.* **2010**, *5*, 5.

(13) Ertl, G. *Angew. Chem., Int. Ed.* **2008**, *47*, 3524.

(14) Zheng, X. X.; Liu, Q.; Jing, C.; Li, Y.; Li, D.; Luo, W. J.; Wen, Y. Q.; He, Y.; Huang, Q.; Long, Y. T.; Fan, C. H. *Angew. Chem., Int. Ed.* **2011**, *50*, 11994.

(15) Zhang, F.; Nangreave, J.; Liu, Y.; Yan, H. *J. Am. Chem. Soc.* **2014**, *136*, 11198.

(16) (a) Brenner, A.; Emmett, P. H. *J. Catal.* **1982**, *75*, 410. (b) Somorjai, G. A.; Beaumont, S. K.; Alayoglu, S. *Angew. Chem., Int. Ed.* **2011**, *50*, 10116.

(17) Herrmann, L. O.; Baumberg, J. J. *Small* **2013**, *9*, 3743−3747.

(18) Henglein, A. *J. Phys. Chem.* **1993**, *97*, 5457.

(19) Mulvaney, P.; Perez-Juste, J.; Giersig, M.; Liz-Marzan, L. M.; Pecharroman, C. *Plasmonics* **2006**, *1*, 61.

(20) Della Pina, C.; Falletta, E.; Prati, L.; Rossi, M. *Chem. Soc. Rev.* **2008**, *37*, 2077.

(21) Bartholomew, C. H. *Appl. Catal., A* **2001**, *212*, 17.

(22) Luo, W. J.; Zhu, C. F.; Su, S.; Li, D.; He, Y.; Huang, Q.; Fan, C. H. *ACS Nano* **2010**, *4*, 7451.

DOI: 10.1021/jacs.5b00324
J. Am. Chem. Soc. 2015, 137, 4292−4295